Journal of Zhejiang University-SCIENCE B (Biomedicine & Biotechnology)
ISSN 1673-1581 (Print); ISSN 1862-1783 (Online)
www.zju.edu.cn/jzus; www.springerlink.com
E-mail: jzus@zju.edu.cn

Science Letters:

A tasseled cap transformation for CBERS-02B CCD data*

Li SHENG[1,2], Jing-feng HUANG[†‡1,2], Xiao-lu TANG[3]

([1]*Institute of Agricultural Remote Sensing and Information Application, Zhejiang University, Hangzhou 310029, China*)

([2]*Key Laboratory of Agricultural Remote Sensing and Information System of Zhejiang Province, Hangzhou 310029, China*)

([3]*Yuhang Branch Bureau of Planning, Hangzhou Urban Planning Bureau, Hangzhou 311100, China*)

[†]E-mail: hjf@zju.edu.cn

Received Mar. 21, 2011; Revision accepted July 26, 2011; Crosschecked Aug. 18, 2011

Abstract: The tasseled cap transformation of remote sensing data has been widely used in agriculture, forest, ecology, and landscape. In this paper, tasseled cap transformation coefficients appropriate for data from a new sensor (China & Brazil Earth Resource Satellite (CBERS-02B)) are presented. The first three components after transformation captured 98% of the four-band variance, and represent the physical characteristics of brightness (coefficients: 0.509, 0.431, 0.330, and 0.668), greenness (coefficients: −0.494, −0.318, −0.324, and 0.741), and blueness (coefficients: 0.581, −0.070, −0.811, and 0.003), respectively. We hope these results will enhance the application of CBERS-02B charge-coupled device (CCD) data in the areas of agriculture, forest, ecology, and landscape.

Key words: Tasseled cap transformation, CBERS-02B CCD, Reflectance factor
doi:10.1631/jzus.B1100088 **Document code:** A **CLC number:** S127

1 Introduction

The tasseled cap transformation has provided a mechanism for data volume reduction and enhanced data interpretability by emphasizing the structures in the multispectral imagery (Crist, 1985). The transformation is sensor-dependent, which means that the transformation coefficients for one sensor cannot be applied successfully to another sensor. The tasseled cap transformation was first applied to Landsat multispectral scanner (MSS) data (Kauth and Thomas, 1976), but has been extended to other sensors, e.g., thematic mapper (TM) (Crist and Cicone, 1984; Crist, 1985), enhanced thematic mapper plus (ETM+) (Huang *et al.*, 2002), IKONOS (Horne, 2003), and moderate-resolution imaging spectroradiometer (MODIS) (Zhang *et al.*, 2002; Lobser and Cohen, 2007).

The tasseled cap transformation turns original, highly covariant data into three uncorrelated indices called brightness, greenness, and wetness (the third tasseled cap transformation components for MSS was called yellow stuff), which can reflect the state of vegetation and soil. In recent years, these three indices have been widely studied and successfully used in studies of agriculture, forest, ecology, and landscape. For instance, the wetness component was used to characterize the dynamics of irrigated crops (Serra and Pons, 2008); tasseled cap indices were used to estimate the age of forest (Wulder *et al.*, 2004); tasseled cap indices can improve the accuracy of mapping and land cover classification (Dymond *et al.*, 2002); a linear combination of tasseled cap indices called the disturbance index can produce significantly more accurate disturbance maps in Russia (Healey *et al.*, 2005); and, wetness and brightness indices were proven to reflect qualitatively both fuel moisture and its distribution, the most important determinants of fire propagation in savanna areas (Mbow *et al.*, 2004).

China & Brazil Earth Resource Satellite (CBERS)-02B was launched in September 2007 in China. The sensor charge-coupled device (CCD) carried by CBERS-02B obtains five bands (one panchromatic band and four multispectral bands) with 19.5 m spatial resolution. In this paper, we aim to present a tasseled cap transformation coefficient appropriate for CBERS-02B CCD data.

‡ Corresponding author

* Project (No. 40871158/D0106) supported by the National Natural Science Foundation of China

2 Materials and methods

2.1 Preparation of CBERS-02B CCD data

The relative spectral response curves of CBERS-02B CCD data are shown in Fig. 1. The CBERS-02B CCD data can be downloaded from the website http://www.cresda.com for free. The level 2 products employed in our study were radiometrically and geometrically corrected and provided by the China Centre for Resources Satellite Data and Application. We selected 10 scenes of CBERS-02B CCD data that captured a variety of land cover types and growing stages. The data preprocessing consisted of two major steps. First, we converted the raw digital number (DN) values to at-sensor radiance. Calculation of at-sensor spectral radiance is necessary in order to normalize the data into a physically meaningful radiometric scale (Chander *et al.*, 2009) that also compensates for the temporal variation of irradiance that can adversely affect the derived tasseled cap values (Huang *et al*., 2002). Second, atmospheric correction was performed using a 6S model. The 6S input parameters include geographic conditions (acquisition date, sun zenith, sun azimuth, viewing zenith, and viewing azimuth), atmospheric conditions, aerosol model, ground visibility, target altitude, sensor altitude, spectral band conditions, ground reflectance characteristics, and atmospheric correction mode. The 10-scene data information and main 6S parameters are listed in Table 1. Geographic conditions were from data information file; ground visibility was from meteorological data; target altitude was from digital elevation model (DEM); and, spectral band conditions were defined by the user.

The following equation is used to covert DN value to at-sensor spectral radiance:

$$L=\mathrm{DN}/a, \tag{1}$$

where L is spectral radiance at the sensor's aperture [W/(m^2·sr·μm)]; DN is digital number value of level 2 product; and, a is the calibration coefficient from the data information file.

The top-of-atmosphere (TOA) is computed as follows:

$$\rho_{\mathrm{TOA}}=\pi LD^2/(E\cos\theta), \tag{2}$$

where ρ_{TOA} is TOA reflectance (unitless); π is mathematical constant ≈3.14159 (unitless); L is spectral radiance at the sensor's aperture [W/(m^2·sr·μm)]; D is Earth-Sun distance (astronomical unit); E is mean exoatmospheric solar irradiance [W/(m^2·μm)], shown in Table 2; and, θ is solar zenith angle (°).

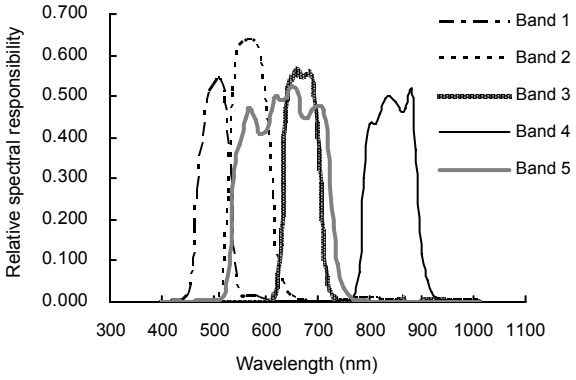

Fig. 1 Relative spectral response curve of CBERS-02B CCD data

Table 1 Data information and main 6S input parameters

Path	Row	Geographic location	Acquisition data	6S input parameter		
				Atmospheric model	Aerosol model	Ground reflectance
367	65	Suzhou	Nov. 29, 2008	Midlatitude winter*	Continental	Non-homogenous
367	65	Suzhou	June 29, 2008	Midlatitude summer*	Continental	Non-homogenous
370	64	Chaohu	Nov. 20, 2008	Midlatitude winter*	Continental	Non-homogenous
370	64	Chaohu	Jan. 11, 2009	Midlatitude winter*	Continental	Non-homogenous
373	55	Huairou	Apr. 17, 2008	US62#	Continental	Non-homogenous
373	55	Huairou	Sept. 22, 2009	US62#	Continental	Non-homogenous
1	55	Beijing	Aug. 22, 2008	Midlatitude summer*	Urban	Non-homogenous
1	55	Beijing	Dec. 30, 2008	Midlatitude winter*	Urban	Non-homogenous
373	66	Wuhan	May 13, 2008	Midlatitude summer*	Urban	Non-homogenous
373	66	Wuhan	Nov. 11, 2008	Midlatitude winter*	Urban	Non-homogenous

Study shows that the atmospheric model in the region of latitude about 40° N in China is close to US62, so here we chose US62 for Huairou in spring and autumn; * The scene locates in the midlatitude area in summer or winter

Table 2 Mean exoatmospheric solar irradiance (*E*) for CBERS-02B CCD

Band	E (W/(m^2·μm))	Band	E (W/(m^2·μm))
1	1919	4	1042
2	1812	5	1636
3	1523		

From http://www.cresda.com

In the 6S model, the relationship between TOA reflectance and target reflectance can be expressed as:

$$\rho_{\mathrm{TOA}}(\theta_{\mathrm{S}},\theta_{\mathrm{V}},\phi_{\mathrm{S}}-\phi_{\mathrm{V}})=\rho_a(\theta_{\mathrm{S}},\theta_{\mathrm{V}},\phi_{\mathrm{S}}-\phi_{\mathrm{V}})+\frac{\rho}{1-\rho S}T(\theta_{\mathrm{S}})T(\theta_{\mathrm{V}}), \quad (3)$$

where θ_{S}, θ_{V}, ϕ_{S}, and ϕ_{V} are solar zenith angle, view zenith angle, solar azimuthal angle, and view azimuthal angle, respectively; $\rho_{\mathrm{TOA}}(\theta_{\mathrm{S}},\theta_{\mathrm{V}},\phi_{\mathrm{S}}-\phi_{\mathrm{V}})$ is TOA reflectance; $\rho_a(\theta_{\mathrm{S}},\theta_{\mathrm{V}},\phi_{\mathrm{S}}-\phi_{\mathrm{V}})$ is path radiance reflectance; ρ is the reflectance of target; S is the spherical albedo of the atmosphere; $T(\theta_{\mathrm{S}})$ is the total downward transmittance; and, $T(\theta_{\mathrm{V}})$ is the total upward transmittance.

2.2 Method of tasseled cap transformation

The basic idea of tasseled cap transformation is compressing spectral data into a few bands associated with physical scene characteristics. Principal component analysis is frequently used to evaluate the data dimensionality. The first two principal components will define a plane very similar to the tasseled cap transformation, and can be rotated to provide features essentially equivalent to the tasseled cap features (Crist and Cicone, 1984). As a first step, principal component transformation coefficients of the 10 scenes containing Bands 1–4 were calculated in ENVI4.3, and a general set of vectors was calculated to determine the initial axes. The approach was to calculate least-squares fitting of the 10 principal component transformation coefficients by minimizing the residual sum of squares (χ):

$$\chi=\sum_{A=1}^{10}\sum_{i=1}^{4}\sum_{j=1}^{4}(PC_{ij}^{A}-R_{ij})^2. \quad (4)$$

The matrix $\boldsymbol{R}$ is a unitary matrix. The matrix $\boldsymbol{PC}^{A}$ is principal component transformation coefficients for Image *A*.

The second step was to rotate the initial axes to the tasseled cap features. At early stage, this was an exploratory, visual process that Crist and Cicone (1984) described rotation method in this way: "these components were then rotated, two or three at a time, in a linear fashion which preserved the orthogonality of the six components. By the process of applying various rotations, the data relationships in the TM data space were discovered and defined." It is obvious that when determining the tasseled cap transformation for a new sensor by this method, the rotating is deemed most appropriate by the investigator. Lobser and Cohen (2007) put forward that the TM tasseled cap transformation is so widely used and well established that it can be referenced as rotation standards which are developed through the relationship between tasseled cap features and their corresponding biophysical parameters. Thus, the process of rotation we adopted was visually interpreted by reference to the TM tasseled cap. First, based on prior knowledge regarding important scene characteristics or data structures of tasseled cap transformation (Table 3) and considering the fourth component was mainly

Table 3 Data structures of tasseled cap transformation about different sensors

Sensor	Band width (μm)					Tasseled cap tranformation result		
	Blue	Green	Red	NIR	SWIR	TC_1	TC_2	TC_3
MSS		0.50–0.60	0.60–0.70	0.70–0.80, 0.80–1.10		Brightness	Greenness	Yellowness
TM/ETM+	0.45–0.52	0.52–0.60	0.63–0.69	0.76–0.90	1.55–1.75, 2.08–2.35	Brightness	Greenness	Wetness
IKONOS	0.44–0.51	0.51–0.59	0.63–0.70	0.78–0.85		Brightness	Greenness	Undefined
MODIS	0.46–0.48	0.54–0.56	0.62–0.67	0.84–0.87, 1.23–1.25	1.63–1.65, 2.10–2.15	Brightness	Greenness	Wetness
CBERS-02B	0.45–0.52	0.52–0.59	0.63–0.69	0.77–0.89				

MSS: multispectral scanner; TM: thematic mapper; ETM+: enhanced thematic mapper plus; MODIS: moderate-resolution imaging spectroradiometer; CBERS: China & Brazil Earth Resource Satellite; NIR: near-infrared; SWIR: short wave-infrared; TC: tasseled cap transformation component

noise, we made assumptions that brightness and greenness can be obtained and tried to find the characteristics for the third component. Second, tasseled cap indices would discriminate different land cover types, and an attempt had been made to represent a wide variety of land cover types in the TM tasseled cap. Hundreds of vegetation, water, soil, and manmade material samples were selected from each scene to guide the rotation process.

To make this method easily understood, here we assumed a three-dimensional (3D) space to illustrate the process of transformation (Fig. 2). The original data with three bands ρ_1, ρ_2, and ρ_3, after principal component transformation, are turned into PC_1, PC_2, and PC_3 (the first, second, and third principal components, respectively). PC_3 is mainly noise, so rotations were performed in the plane of PC_1-PC_2 with the orthogonality of PC_3 axis. Under the guide of samples, angle θ rotation is applied to shift PC_1 and PC_2 axes to TC_1 and TC_2 axes (the first and second tasseled cap transformation components).

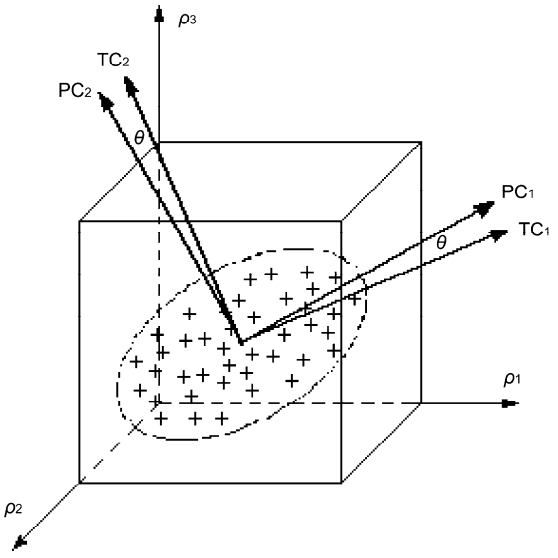

Fig. 2 Illustration of transformation process

ρ_1, ρ_2, and ρ_3 are the original data axes; PC_1 and PC_2 are the initial axes after transformation; TC_1 and TC_2 are the final axes after a series of rotations (θ) of PC_1 and PC_2

In the course of PC axes to TC axes, rotations are applied in a 3D space (the fourth component was mainly noise) which preserves the orthogonality of three axes. A series of small angle rotations were made based on the following equations:

$$(R_1', R_2', R_3', 1) = (R_1, R_2, R_3, 1)\begin{bmatrix} \cos\gamma & \sin\gamma & 0 & 0 \\ -\sin\gamma & \cos\gamma & 0 & 0 \\ 0 & 0 & 1 & 0 \\ 0 & 0 & 0 & 1 \end{bmatrix},$$

$$(R_1', R_2', R_3', 1) = (R_1, R_2, R_3, 1)\begin{bmatrix} 1 & 0 & 0 & 0 \\ 0 & \cos\alpha & \sin\alpha & 0 \\ 0 & -\sin\alpha & \cos\alpha & 0 \\ 0 & 0 & 0 & 1 \end{bmatrix},$$

$$(R_1', R_2', R_3', 1) = (R_1, R_2, R_3, 1)\begin{bmatrix} \cos\beta & 0 & \sin\beta & 0 \\ 0 & 1 & 0 & 0 \\ -\sin\beta & 0 & \cos\beta & 0 \\ 0 & 0 & 0 & 1 \end{bmatrix},$$

where R_1', R_2', and R_3' are the axis coefficients after angle rotation of the original axis coefficients R_1, R_2, and R_3; and α, β, and γ are rotation angles in three planes, respectively.

3 Results and discussion

3.1 Analysis of CCD data

The CBERS-02B CCD relative spectral response curves show that there are overlaps between the multispectral bands (Fig. 1), which means that they have correlations. The correlation coefficients among the four multispectral bands of the 10 scenes of CCD data were calculated, and the means of these correlations are shown in Table 4. Note that there are high correlations among the three visible region bands (ρ_1, ρ_2, and ρ_3), while ρ_4 in the near-infrared (NIR) region is substantially less correlated with the other bands. These moderate to high inter-band correlations demonstrate that there is a lot of redundancy in the original CCD data. The tasseled cap transformation components are uncorrelated and contain enhanced biophysical information.

Table 4 Mean correlation coefficients among the four multispectral bands

Reflectance	Correlation coefficient			
	ρ_1	ρ_2	ρ_3	ρ_4
ρ_1	1.000	0.980	0.981	0.396
ρ_2	0.980	1.000	0.978	0.477
ρ_3	0.981	0.978	1.000	0.417
ρ_4	0.396	0.477	0.417	1.000

3.2 Tasseled cap transformation components

Table 5 gives the tasseled cap transformation coefficients for CBERS-02B CCD data based on reflectance factor. The first three components can extract 98% of the total variance of the original data and represent the physical characteristics of brightness (TC_1), greenness (TC_2) and blueness (TC_3), respectively.

Table 5 Tasseled cap transformation coefficients for CBERS-02B CCD data

Component	Coefficient			
	ρ_1	ρ_2	ρ_3	ρ_4
TC_1	0.509	0.431	0.330	0.668
TC_2	−0.494	−0.318	−0.324	0.741
TC_3	0.581	−0.070	−0.811	0.003
Fourth	−0.449	0.845	−0.285	−0.051

Brightness (TC_1) is the weighted sum of four bands, but is dominated by the contribution from the near-infrared (NIR) band.

Greenness (TC_2) is the contrast between the three visible bands and the NIR band, which captures the characteristic green vegetation reflectance pattern: high absorption and low reflectance in the visible bands contrasted with the high reflectance in the NIR band.

Blueness (TC_3), this component contrasts strong blue reflectance and strong red absorptance. The very weak contributions from the green and NIR bands more or less cancel one another. The blue plastic roof (Fig. 3), due to its high reflectance in the blue band and high absorption in the other bands, shows brightest in TC_3.

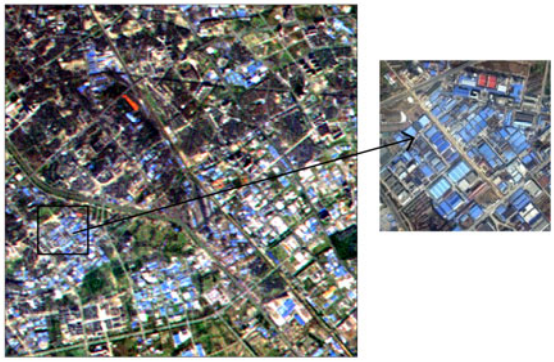

Fig. 3 Blue plastic roof in the CBERS-02B image

3.3 Discussion of the tasseled cap transformation

A 400×400 extract from the CBERS-02B CCD image of the Suzhou area, acquired in November 2008, is shown as an example to explain the tasseled cap transformation results (Fig. 4). Both TC_1 (Fig. 4a) and the panchromatic image (Fig. 4d) display similar physical characteristics—object brightness, but TC_1 enhances the contrast of the data and eliminates noise compared to the panchromatic image. The CBERS-02B panchromatic band captures very little radiance from the blue and NIR portions of the spectrum. TC_1, on the other hand, is dominated by NIR radiance with a strong contribution from the blue band. In TC_1, buildings tend to be bright, dense vegetation is intermediate, and water is dark. In TC_2 (Fig. 4b), vegetation tends to be bright, while buildings and water are both dark. In TC_3 (Fig. 4c), the blue plastic roofs (Fig. 3), mainly in the industrial area, appear the brightest in TC_3.

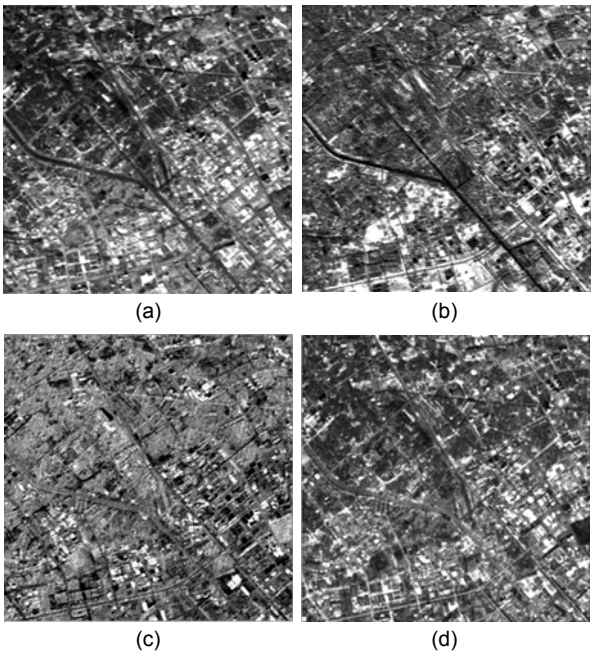

Fig. 4 A 400×400 extract from CBERS-02B CCD image of Suzhou area in November, 2008
(a) TC_1; (b) TC_2; (c) TC_3; (d) Panchromatic image

The 2D scatter diagrams of Figs. 4a–4c are illustrated in Fig. 5a. Several key land cover types are plotted on these three planes in Fig. 5b.

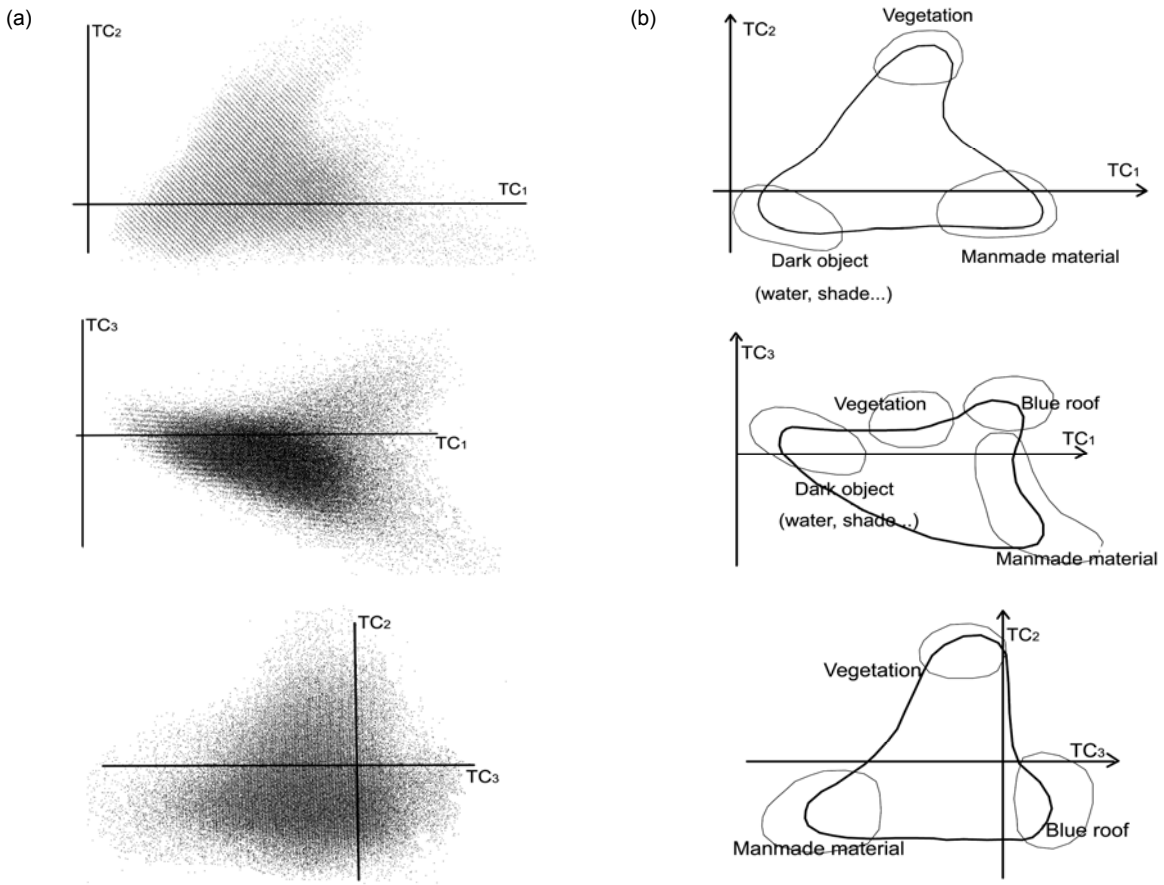

Fig. 5 CBERS-02B tasseled cap transformation data of Figs. 4a–4c (a) and the corresponding land cover types (b)

4 Conclusions

An appropriate suggested set of tasseled cap transformation coefficients for the CBERS-02B CCD data is presented. The transformation is based on reflectance factor. The first three components after transformation capture 98% of the four-band variance, and represent the physical characteristics of brightness, greenness, and blueness, respectively. We hope these results will enhance the application of CBERS-02B CCD data in the areas of agriculture, forest, ecology, and landscape.

Acknowledgements

The authors wish to express a gratitude to the China Centre for Resources Satellite Data and Application for CBERS-02B level 2 data.

References

Chander, G., Markham, B.L., Helder, D.L., 2009. Summary of current radiometric calibration coefficients for Landsat MSS, TM, ETM+, and EO-1 ALI sensors. *Remote Sens. Environ*., **113**(5):893-903. [doi:10.1016/j.rse.2009.01.007]

Crist, E.P., 1985. A TM tasseled cap equivalent transformation for reflectance factor data. *Remote Sens. Environ.*, **17**(3): 301-306. [doi:10.1016/0034-4257(85)90102-6]

Crist, E.P., Cicone, R.C., 1984. A physically-based transformation of Thematic Mapper data—the TM tasseled cap. *IEEE Trans. Geosci. Remote Sens.*, **22**(3):256-263. [doi: 10.1109/TGRS.1984.350619]

Dymond, C.C., Mladenoff, D.J., Radeloff, V.C., 2002. Phenological differences in tasseled cap indices improve deciduous forest classification. *Remote Sens. Environ.*, **80**(3):460-472. [doi:10.1016/S0034-4257(01)00324-8]

Healey, S.P., Cohen, W.B., Yang, Z.Q., Krankina, O.N., 2005. Comparison of tasseled cap-based Landsat data structures for use in forest disturbance detection. *Remote Sens. Environ*., **97**(3):301-310. [doi:10.1016/j.rse.2005.05.009]

Horne, J.H., 2003. A Tasseled Cap Transformation for IKONOS Images. ASPRS Annual Conference Proceedings. Alaska, USA.

Huang, C., Wyli, B., Yang, L., Homer, C., Zylstra, G., 2002. Derivation of a tasseled cap transformation based on Landsat 7 at-satellite reflectance. *Int. J. Remote Sens.*, **23**(8):1741-1748. [doi:10.1080/01431160110106113]

Kauth, R.J., Thomas, G.S., 1976. The Tasseled Cap—A Graphic Description of the Spectral-Temporal Development of Agricultural Crops as Seen by Landsat. Proceedings of the Symposium on Machine Processing of Remotely Sensed Data. West Lafayette, Indiana, p.41-51.

Lobser, S.E., Cohen, W.B., 2007. MODIS tasselled cap: land cover characteristics expressed through transformed MODIS data. *Int. J. Remote Sens.*, **28**(22):5079-5101. [doi:10.1080/01431160701253303]

Mbow, C., Goıta, K., Benie, G.B., 2004. Spectral indices and fire behaviour simulation for fire risk assessment in savanna ecosystems. *Remote Sens. Environ.*, **91**(1):1-13. [doi:10.1016/j.rse.2003.10.019]

Serra, P., Pons, X., 2008. Monitoring farmers' decisions on Mediterranean irrigated crops using satellite image time series. *Int. J. Remote Sens.*, **29**(8):2293-2316. [doi:10.1080/01431160701408444]

Wulder, M.A., Skakun, R.S., Kurz, W.A., White, J.C., 2004. Estimating time since forest harvest using segmented Landsat ETM+ imagery. *Remote Sens. Environ.*, **93**(1-2):179-187. [doi:10.1016/j.rse.2004.07.009]

Zhang, X.Y., Schaaf, C.B., Friedl, M.A., Strahler, A.H., Gao, F., Hodges, J.F.C., 2002. MODIS Tasseled Cap Transformation and Its Utility. Proceedings of the International Geosciences and Remote Sensing Symposium. Toronto, Canada, p.1063-1065.